PERFORMANCE ASPECTS OF DE LAVAL SPRAY-FORMING NOZZLES

Kevin M. McHugh and James F. Key
Idaho National Engineering Laboratory
Idaho Falls, ID

ABSTRACT

Spray forming is a multiphase fabrication technology in which a spray of finely atomized liquid droplets is directed onto a suitably shaped substrate or pattern to produce a coherent, near-net-shape deposit. The technology can simplify materials processing while simultaneously improving product quality. Researchers at the Idaho National Engineering Laboratory (INEL) are developing spray-forming technology for producing near-net-shape solids and coatings of a variety of metals, polymers, and composite materials using de Laval nozzles. Here we briefly describe the flow field characterization and atomization behavior of liquid metals in linear de Laval nozzles, and illustrate their versatility by summarizing results from three spray-forming programs. In one program, low-carbon steel strip >0.75 mm was produced. In another program, polymer membranes ~ 5 μm thick were spray formed. Finally, recent results in spray forming molds, dies, and related tooling for rapid prototyping are described.

INTRODUCTION

Spray forming is a multiphase fabrication technology in which a spray of finely atomized liquid droplets is deposited onto a suitably shaped substrate or pattern to produce a coherent solid. The technology offers unique opportunities for simplifying materials processing without sacrificing product quality. In fact, spray forming oftentimes substantially improves product quality. The technology has near-net-shape fabrication capabilities, is applicable to a wide range of metals and nonmetals, and offers property improvements through rapid solidification, e.g., refined microstructures, extended solid solubilities, and reduced segregation. Economic benefits result from process simplification and the elimination of unit operations.

Researchers at the Idaho National Engineering Laboratory (INEL) are developing spray-forming technology using linear de Laval (converging/diverging) nozzle designs to produce solids and coatings of a variety of materials. The approach combines unique spray nozzle designs with on-line diagnostics of the spray plume and product quality. An in-flight particle diagnostics system is used to simultaneously measure single particle size, velocity, and temperature in the atomized plume. This system measures particle diameters between 5 and 1,000 μm using an absolute magnitude of scattered light technique. Velocities of 10 to 100 m/s are measured with a dual beam laser Doppler velocimeter, and particle temperature is measured with a high-speed two-color pyrometry technique. Guidance for component design and process control is provided by modeling efforts in multiphase flow, heat transfer, and solidification phenomena.

During operation, the spray nozzle generates a low static pressure region near the nozzle's throat. Metals, polymers, and composite materials have been spray formed by aspirating or pressure feeding the liquid through a slit orifice or a series of circular orifices that span the width of the nozzle. A high-velocity, high-temperature inert gas atomizes the liquid; the resultant droplets are entrained by the gas stream and deposited onto a substrate. For metals, in-flight convection cooling of the droplets followed by conduction, convection, and radiation cooling at the substrate results in rapid solidification of the deposit. This restricts grain growth and improves product homogeneity by reducing the segregation of impurities. The shape of the spray-formed object is largely dictated by the geometry of the substrate or pattern onto which the spray is deposited, allowing complex shapes to be readily produced. Figure 1 illustrates the rapid solidification and near-net-shape qualities of this approach. The semispherical shell was generated by spray-depositing molten tin directly onto an inflated party balloon.

Results from several INEL spray-forming programs are described to illustrate the flexibility of the approach. These programs involved spray forming low-carbon steel strip, complex metal shapes using low melting point alloys, and polymer

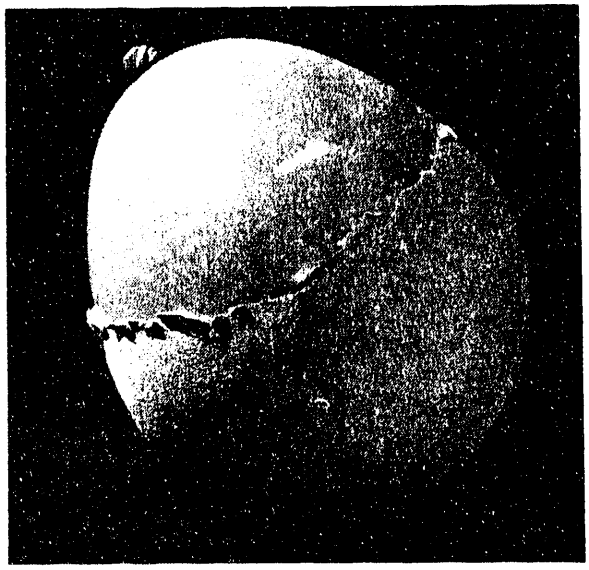

FIG. 1. PARTY BALLOON SPRAY-COATED WITH TIN EMPHASIZES RAPID SOLIDIFICATION AND NEAR-NET-SHAPE CAPABILITY OF SPRAY FORMING.

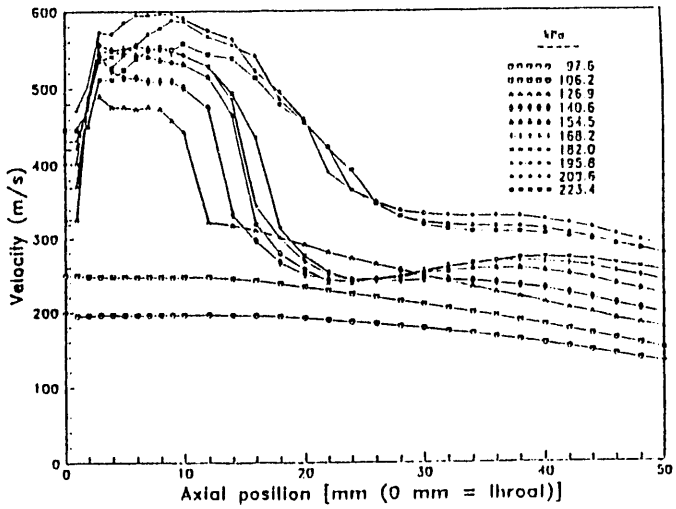

FIG. 2. MEASURED GAS VELOCITY ALONG CENTERLINE OF NOZZLE AT TWELVE INLET PRESSURES.

membranes. As a backdrop to these results, a description of the atomization behavior and flow field characteristics of INEL-designed de Laval spray-forming nozzles is given.

ATOMIZATION AND NOZZLE FLOW FIELD CHARACTERIZATION

Single-Phase Flow Characterization

An understanding of the atomization behavior and characteristics of the flow field are important because the properties of the spray-formed product reflect the interplay of the characteristics of the spray plume (droplet size distribution, velocity, heat content, flux, and flow pattern) and substrate (material properties, surface finish). Fincke et al. have performed gas flow field characterization studies of INEL spray-forming nozzles, and Berry has extensively modeled their single- and multiphase flow behavior [1]. Flow field diagnostics were performed using stagnation and static pressure probes constructed from small diameter hypodermic tubing. The flow field along the center line of the nozzle was mapped by traversing the probes from the center of the throat through the diverging section and into the free jet region. Gas velocities were calculated from static and stagnation pressure measurements using compressible flow theory at twelve nozzle inlet pressures. Figure 2 summarizes results for room temperature argon and a back pressure of about 86 kPa (12.5 psia). Supersonic flows were observed downstream of the throat for nozzle inlet pressures exceeding about 120 kPa (17.5 psia). The supersonic flow region extended about 10 mm before it began to shock down through what is believed to be a series of weak oblique shocks. The flow was driven to supersonic velocity outside the nozzle, with nozzle inlet pressures in excess of approximately 223 kPa (32 psia).

The flow field was also mapped at the nozzle's exit plane. Results for the velocity profile are given in Figure 3. The

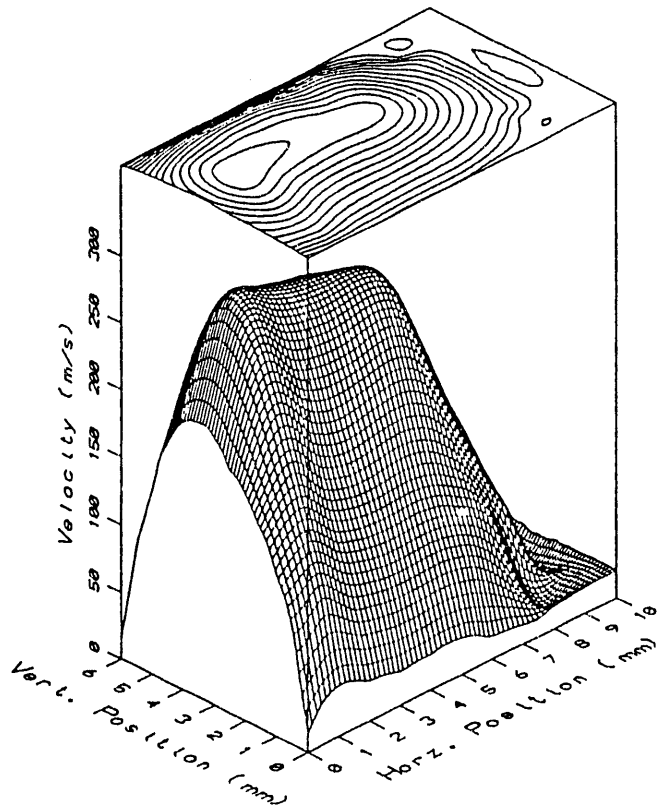

FIG. 3. VELOCITY PROFILE AT EXIT PLANE OF NOZZLE.

profile is symmetric, with no indication of flow separation. Flow separation has been observed and has been computationally predicted by Berry [1], in nozzles with excessively large diver-

DISCLAIMER

gence angles. This undesirable condition is avoided as much as possible, since it can result in poor atomization performance in terms of large average droplet size and a broad distribution of droplet sizes.

De Laval spray-forming nozzles can be operated by aspirating or pressure feeding liquid into the flow channel through one or more liquid orifices. In the aspirating mode, many important characteristics of the spray plume, such as mass loading, mass distribution in the spray, and spray divergence, depend on the magnitude and uniformity of suction, i.e., the difference between atmospheric pressure and local static pressure at the liquid orifices. These differences, in turn, are dictated by the geometry of the nozzle. Most important in this regard are entrance and exit angles, throat dimensions, size and location of the liquid orifices, and contour of the flow channel near the orifices. For a given nozzle geometry, the magnitude and uniformity of suction then depends on atomizing gas, flow conditions, and gas temperature.

The magnitude and uniformity of suction at the liquid orifices were evaluated using static pressure probes placed perpendicular to the flow direction. Results using room temperature argon and a back pressure of 86 kPa (12.5 psia) are given in Figure 4. The local static pressure measured at each of six liquid orifices is plotted against the nozzle inlet pressure, giving rise to the envelope of curves. The curve profiles are parabolic-like; the pressure at the liquid orifices decreased with increasing nozzle inlet pressure from atmospheric pressure to a minimum and then increased again. The well depth, which corresponds to the magnitude of the suction, is approximately 42 kPa (6 psia). Above an inlet pressure of approximately 200 kPa (29 psia), the pressure at the liquid orifices rises above atmospheric pressure. In the aspiration mode, the net driving pressure for a liquid is the sum of the liquid pressure head and suction pressure contributions. During operation, the nozzle inlet pressure can be increased to hold back the flow of liquid, thus providing a simple way to start/stop the spray.

The suction uniformity is best at lower nozzle pressures. At high flows, the individual curves diverge, with a larger reduction in suction at liquid orifices nearest the side walls (L.O. #1 and L.O. #6 in Figure 4) due to drag effects.

As the nozzle wall and atomizing gas temperatures were increased, the depth of the well in Figure 4 decreased, the well broadened, and the minimum was shifted slightly to lower nozzle inlet pressures. A given nozzle typically exhibited a logarithmic-like dependence of suction with temperature, with a decrease in suction of about 25% as the operating temperature was increased from 300 to 1,875 K. This was largely due to the increase in gas viscosity.

Atomization Behavior

During gas atomization, a liquid is disintegrated into relatively fine droplets by the action of aerodynamic forces that overcome surface tension forces that consolidate the liquid [2]. The liquid's viscosity and density also influence atomization behavior, but they typically play a more secondary role. Viscosity affects both the degree of atomization and the spray pattern by influencing the amount of interfacial contact area between the liquid and gas. Viscous liquids oppose change in geometry

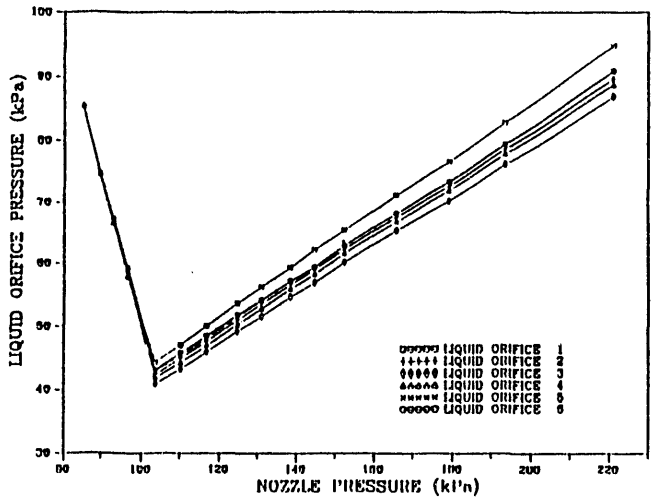

FIG. 4. STATIC PRESSURE AT EACH LIQUID ORIFICE AS A FUNCTION OF INLET PRESSURE.

more efficiently than low viscosity liquids, making the generation of a uniform spray jet more difficult for a given set of flow conditions. Density influences how the liquid responds to momentum transfer from the gas. Light liquids accelerate more rapidly in the gas jet. Disintegration efficiency is reduced because atomization takes place at lower relative velocities.

Liquid metals are characterized by moderately high viscosity, high density, and very high surface tension compared to common liquids such as methanol, water, and acetone. These properties, and the intrinsic high-temperature requirements, make the atomization of liquid metals more difficult than with most liquids. As a result, liquid metal spray-forming nozzles need to be designed to provide good gas/metal coupling with efficient kinetic energy transfer from the gas. In linear de Laval nozzles, the liquid metal enters the flow channel with an axial velocity that is essentially zero. There, it contacts a high-velocity, high-temperature inert gas. High-temperature gas is used to help maintain the liquid metal in a fluid state throughout breakup. Relatively large droplets or sheets form initially, then undergo secondary atomization by various mechanisms, depending upon local flow patterns, flow velocity, mass loading, and the physical properties of the gas and liquid metal.

Dynamics of droplet breakup in high-velocity flows is quite complicated. Historically, the Weber number, "We," has been a useful predictor of breakup tendency [3]. "We" represents the ratio of inertial forces to surface tension forces:

$$We = \frac{\rho V^2 D}{2\sigma}$$

where ρ is the density of the gas, V is the initial relative velocity between the flow field and the drop, D is the initial diameter of the drop, and σ is the surface tension of the drop [4]. Breakup of liquid drops will not occur unless the Weber number exceeds a critical value, We_{crit}. Shock exposure of various liquids has yielded We_{crit} values ranging from about 1 to 25 [5-21]. There are, however, few measured We_{crit} values cited in the literature for liquid metals exposed to high-velocity flows. Haas [20] has

observed We_{crit} to be between 5 and 6 for mercury drops falling vertically into an opposing high-velocity free jet of air. The critical Weber number associated with the atomization of liquid tin in INEL nozzles is estimated to be close to 1 for a nozzle operating at an inlet pressure of 207 kPa (30 psia) absolute, with argon gas heated to 300°C. We_{crit} was calculated for a 14 μm droplet using the surface tension of the bulk liquid at its melting point and the measured gas and droplet flow velocities. The density of the gas was calculated using compressible flow theory. In contrast, the Weber number associated with breakup of a 3 mm tin droplet at the liquid's injection point is estimated to be about 280 under the same nozzle conditions.

The Ohnesorge number, "On," is useful as a means of predicting the role of viscosity on droplet breakup [3]. Physically, "On" is the ratio of the viscous forces to the product of inertial and surface tension forces of a drop:

$$On = \frac{\mu_d}{(\rho_d D \sigma)^{1/2}}$$

where μ_d and ρ_d are the dynamic viscosity and density of the drop [4]. If $O_n < 1$, viscous effects are secondary. For values larger than 1, the effect of viscosity is to increase the value of We_{crit} required for breakup [3]. On is calculated to be < 1 for 14 μm and 3 mm tin droplets at the melting point of tin.

Atomization usually proceeds through stages, producing a range of droplet sizes. Fincke et al. [1] have applied high-speed video techniques to examine metal breakup in INEL nozzles and have observed at least two breakup mechanisms, depending upon the flow conditions and mass loading. One of these, termed "bag breakup," was observed at low nozzle inlet pressures. "Bag breakup" has been observed in a number of studies on a variety of liquids in both steady and transient flow fields. Pilch and Erdman [4] have correlated this type of breakup and the related "bag and stamen breakup," with initial Weber numbers 12 < We < 100. In "bag breakup," the center portion of a drop's front surface first becomes concave and then is blown out downstream to form a hollow bag attached to a more massive torroidal rim. The bag bursts, producing a shower of relatively fine droplets and filaments. Surface tension then consolidates the rim into one or more fragments, which can undergo breakup depending upon the Weber number [3].

Another breakup mechanism, associated with higher initial Weber numbers (100 < We), has also been observed in these nozzles. This mechanism is termed "stripping" ("sheet stripping" and "wave crest stripping" are examples) and occurs when a droplet deforms in a manner nearly opposite to "bag breakup." The drop flattens on the downstream side and presents a convex surface to the flow. Depending on the relative velocity and physical properties of the liquid, the edges of the deformed drop elongate into sheets and fine filaments or drops which later detach.

Examination of unconsolidated powders collected during spray forming with de Laval nozzles provides insight into the breakup mechanisms taking place. Normally, an abundance of spherical or near-spherical shapes are found as the scanning electron microscope (SEM) photograph in Figure 5a illustrates. Other shapes have been observed, however. For example, the intermixing of prolate ellipsoidal particles with fine spherical tin particles in Figure 5b suggests that the former resulted when liquid tin filaments, generated during "bag breakup" or "stripping," solidified in flight. The irregular powder shapes shown in Figure 5c were formed using the same nozzle but at low gas flow rates. These large, irregular shapes are suggestive of parent droplets that began to undergo "bulgy" deformation and breakup, as described by Hinze [21], but were frozen in flight. The bulges and protuberances appear larger than expected, if due solely to solidification shrinkage.

In general, conditions that favor the formation of a narrow droplet size distribution and a small average droplet size are preferred in most spray-forming applications. The size distribution of high purity (99.8% by wt) tin powders collected during spray-forming experiments has been evaluated using wet and dry sieving techniques. The powder was produced using a bench-scale linear de Laval nozzle of our own design having a transverse throat width of 17 mm. The nozzle, which was machined in-house from boron nitride stock, was operated at a pressure of 207 kPa (30 psia), with argon heated to approximately 300°C, as the atomizing gas. Liquid tin was superheated about 70°C above its melting point and pressure-fed into the nozzle through a series of liquid orifice holes that spanned the width of the nozzle. The gas-to-metal mass ratio was about 10, with a metal throughput of approximately 0.5 kg/s per meter of nozzle throat width. The powder was collected in a chamber, passivated, and size-analyzed by sieving through fine mesh screens of 300, 250, 210, 150, 125, 90, 75, 63, 53, 38, 25, 18, 15, 10, and 5 μm. Few particles larger than 125 μm were observed.

Figure 6 is a histogram plot that gives the count frequency distribution versus powder size. The ordinate gives the count frequency normalized for the sieve size range, expressed as a percentage of the total counts. The plot indicates that about 85% of the powder particles were < 5 μm in diameter. The average particle size was 4 μm. The plot in Figure 7 is a histogram plot that relates mass frequency to powder size for the same tin powder sample, again normalized for the size range of the sieves. When compared with Figure 6, this distribution reflects the significance of the mass weighting factors (which go as d^3) imposed by relatively small numbers of more massive particles. Since most spray-forming applications are mass intensive, the distribution in Figure 7 is a more representative description of the powder (and spray plume) size distribution. The Sauter (or area) mean diameter, d_{sm}, and volume mean diameter, d_{vm}, were calculated to be 23 and 31 μm, respectively, using the following equations:

$$d_{sm} = \frac{\sum n_i d_i^3}{\sum n_i d_i^2} \qquad d_{vm} = \frac{\sum n_i d_i^4}{\sum n_i d_i^3}$$

d_{sm} is particularly useful in evaluating droplet sizes for surface area intensive processes such as combustion of fuels and spray drying. It is sensitive to finer droplets, while d_{vm} is sensitive to coarser droplets. Together, they give a balanced view of the powder size. The mass median diameter, d_m, was determined to be 23 μm by interpolation of the cumulative weight versus size data given in Figure 8. It is the diameter corresponding

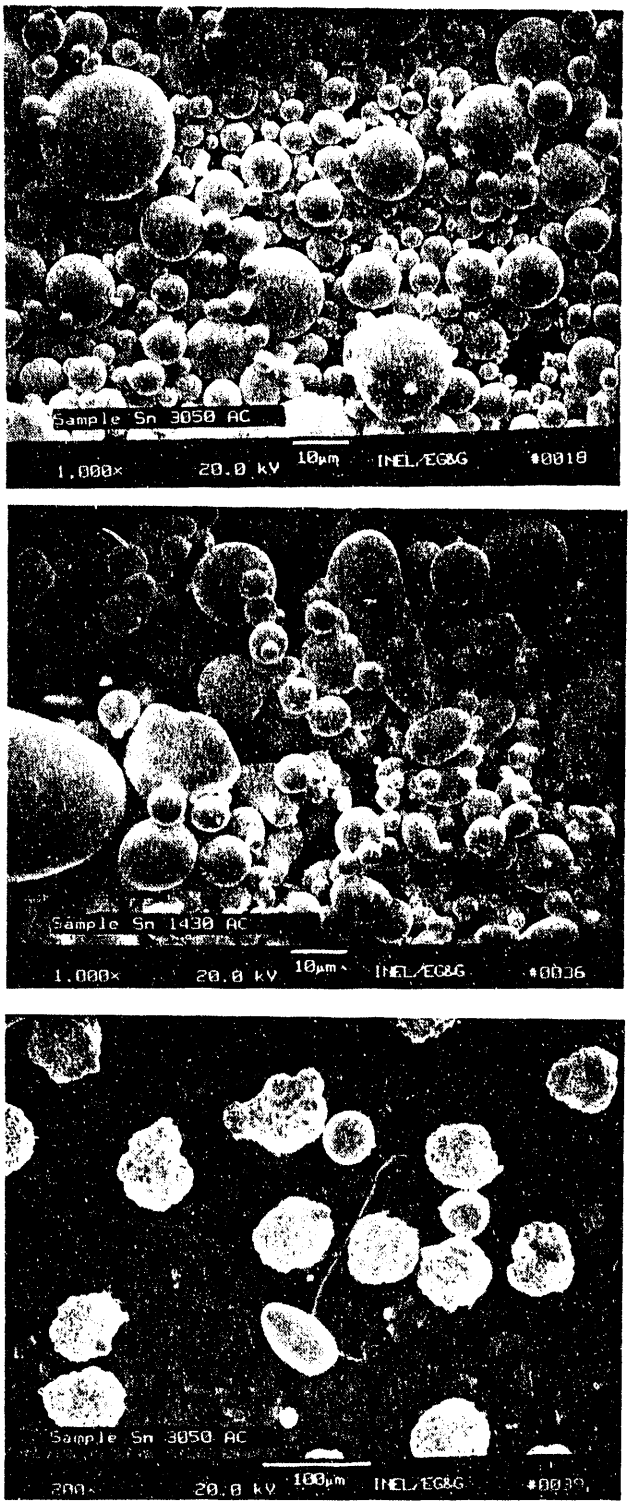

FIG. 5. SEM PHOTOGRAPHS OF TIN POWDER.

with 50% cumulative weight (d_{50}). The geometric standard deviation, $\sigma_v = (d_{84}/d_{16})^{1/2}$, was calculated to be 1.5, indicating a narrow droplet size distribution in the spray plume.

The distribution of particle size in Figure 7 is bimodal,

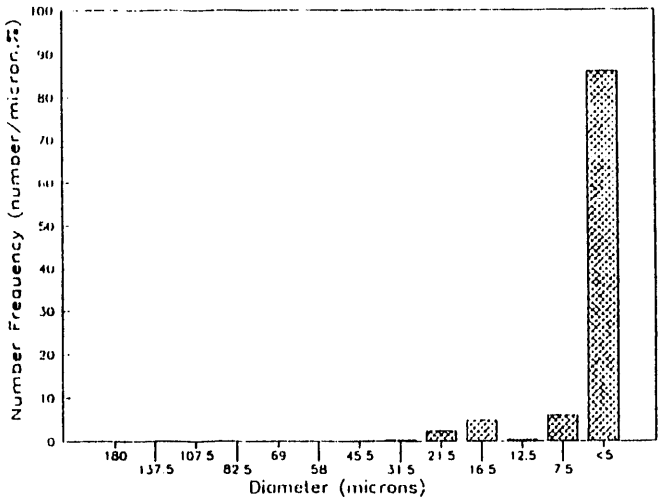

FIG. 6. NUMBER FREQUENCY OF TIN POWDER.

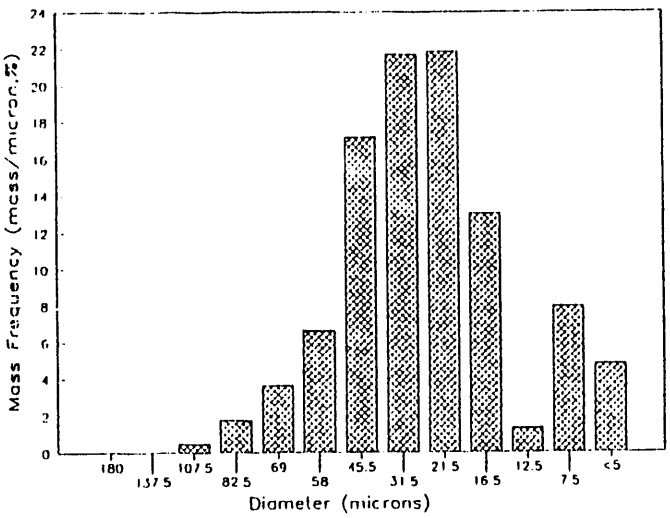

FIG. 7. MASS FREQUENCY OF TIN POWDER.

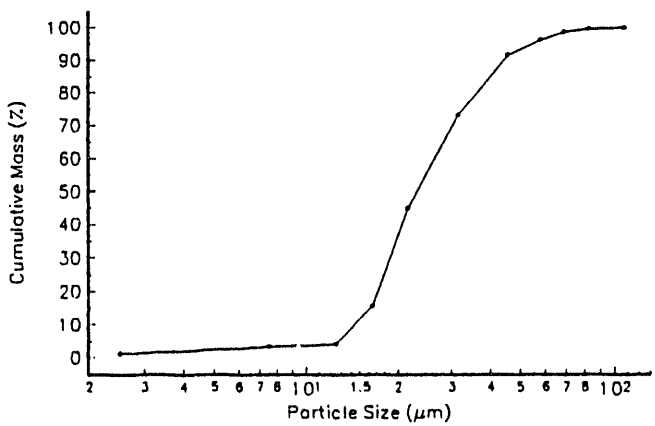

FIG. 8. LOG-NORMAL CUMULATIVE MASS PLOT OF TIN POWDER.

suggesting two families of droplets in the spray plume. Ünal has also observed bimodal size distributions for gas atomized zinc and aluminum powders using a different confined gas atomization nozzle design [22]. The two families have been proposed to correspond with stable and daughter droplets formed by "stripping" mechanisms. The smallest stable droplet size observed, 14 μm, was determined to correspond to a critical Weber number of about 1, as described above.

APPLICATIONS OF SPRAY-FORMING TECHNOLOGY WITH DE LAVAL NOZZLES

Atomized sprays find use in a wide range of applications including spray drying, cooling, combustion, painting, and powdered metal production. Spray forming differs from other applications in that engineered alloys, plastics, and composite materials are spray deposited to generate free standing near-net-shape or net-shape solids and coatings. Properties of the spray-formed product also reflect the interplay of characteristics of the spray plume and substrate onto which the spray is deposited. The INEL is pioneering use of de Laval nozzles in spray forming. In this section, a summary of results from three spray-forming programs are described to illustrate the versatility of the approach and the intrinsic technical and economic advantages it has over conventional approaches. These programs involved the production of low-carbon steel strip, polymer membranes, and spray-formed tooling.

Low-Carbon Steel Strip

Nearly all low-carbon steel strip is produced by conventional ingot or thin-slab metallurgical techniques. Molten steel is cast as an ingot or slab and extensively deformed to obtain the desired shape and properties. This is highly energy intensive and requires large capital investments. In contrast, INEL spray-forming technology transforms molten metal close to final strip form in a single rapid solidification step. Minor hot rolling then fully densifies and further refines the metal's microstructure. This can lead to enormous cost savings. For low-carbon steel hot band, the industry's highest volume commodity, techno-economic analysis estimated improvement in production costs by as much as $50 to $100 per ton. At the current domestic production rate of 50 to 60 million tons per year, this corresponds to cost savings of $2.5 to $6 billion per year. This savings is due primarily to eliminating unit operations and associated energy costs. Improvements in product quality are equally impressive. For example, after hot rolling (~60% thickness reduction), INEL spray-formed low-carbon steel strip typically had about 50% higher yield and ultimate tensile strength than commercial strip; i.e., its properties resemble those of the more costly high-strength low-alloy steels.

The INEL spray-forming approach for producing metal strip is depicted schematically in Figure 9. Gas atomization of a molten metal feedstock is accomplished using a converging-diverging (de Laval) nozzle; the resultant droplets are entrained in a highly directed two-phase flow and deposited onto a rotating, water-cooled drum. Rapid solidification of the deposit restricts grain growth and improves product homogeneity by reducing the segregation of impurities that form inclusions.

Bench-scale linear converging/diverging nozzles of our own design were machined in-house from boron nitride. Interchangeable inserts of high purity Al_2O_3 were used in critical areas to minimize erosion of the boron nitride by the molten steel. The throat width, transverse to the direction of flow, was about 25 mm. Mass throughputs were as high as 43 Mg/h per meter of slit width for a slit orifice nozzle operating in the aspiration mode, and 165 Mg/h per meter for the same nozzle operating in the pressurized feed mode. A purged argon atmosphere within the spray apparatus minimized slag formation in the melt, surface oxidation of the strip, and in-flight oxidation of the atomized droplets.

The nozzle operated at a static pressure of 206 kPa (30 psia) absolute, measured at the nozzle's inlet. The driving pressure was found to generate supersonic flow conditions; the shock front was in the diverging section near the metal feed location. Gas-to-metal mass ratios typically ranged from 0.1 to 0.5. The gas and droplets cooled rapidly after exiting the nozzle as the spray plume entrained cool ambient argon. Gas and droplet velocity also decreased after exiting the nozzle, with large droplets responding less to drag effects by virtue of their greater momentum.

The starting material was remelted SAE 1008 hot band. During a typical run, 1.5 kg of steel was induction heated to about 100°C above the liquidus temperature and atomized using argon heated to about 1,000°C. The resultant droplets impacted a water-cooled, grit-blasted mild steel drum, producing a strip of metal about 127 mm wide x 3 mm thick.

The microstructure of the as-deposited steel was usually fine, equiaxed ferrite with 11 to 45 μm average grain size. Transformation of the microstructure of SAE 1008 steel as it goes from commercial hot band to as-deposited material and finally to hot-rolled product is shown in Figure 10. Note that the average grain size of the as-deposited material is about the same as that of the commercial hot band (~16 μm), but the grains are somewhat more directional, reflecting the heat transfer direction. The grain structure of the spray-formed and hot-rolled material was equiaxed ferrite with ~5 μm grain diameters.

As-deposited density, measured by water displacement using Archimedes' principle, ranged from 88 to 97% of theoretical density, with 96% being typical. Full densification of the as-deposited strip was achieved with standard hot deformation processing. Depending upon the sample, hot rolling at 1,000 to 1,100°C to 30 to 70% thickness reduction was sufficient. Low porosities, together with fine microstructures, were obtained with conditions that favored the formation of dense sprays consisting of small droplets with low solid fractions. The refined and uniform microstructures of thin hot-rolled strip generated under these conditions can be seen in Figure 11.

As expected, the tensile properties of the spray-formed and hot-rolled low-carbon steel strip reflect the observed grain refinements. Table 1 summarizes the results. The range of values arises from differences in processing parameters (particularly spray conditions). Compared to commercial hot band, yield strengths increased 47 to 64% and ultimate strengths increased 9 to 63%. The observed reduction in elongation was largely restored by normalizing the samples (heating to 930°C for ~5 min followed by air cooling). Fully annealed samples (heated to 930°C followed by very slow cooling in the furnace)

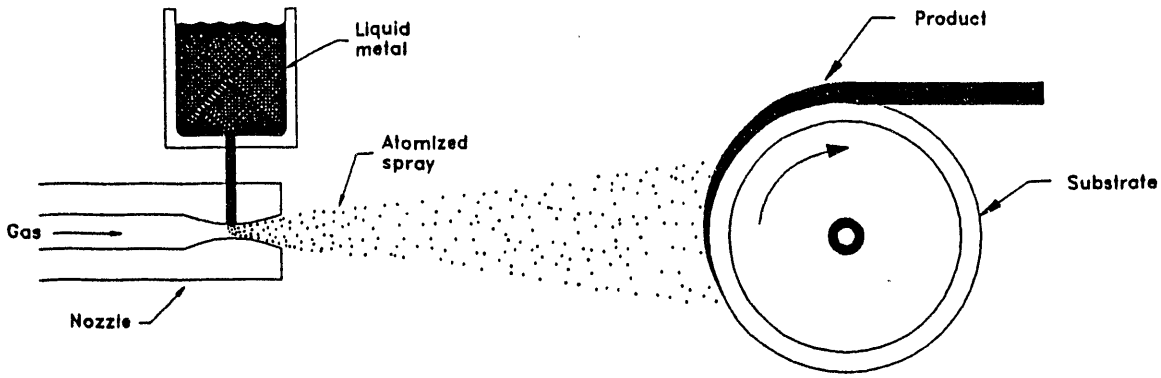

FIG. 9. SCHEMATIC OF APPROACH FOR SPRAY-FORMING METAL STRIP.

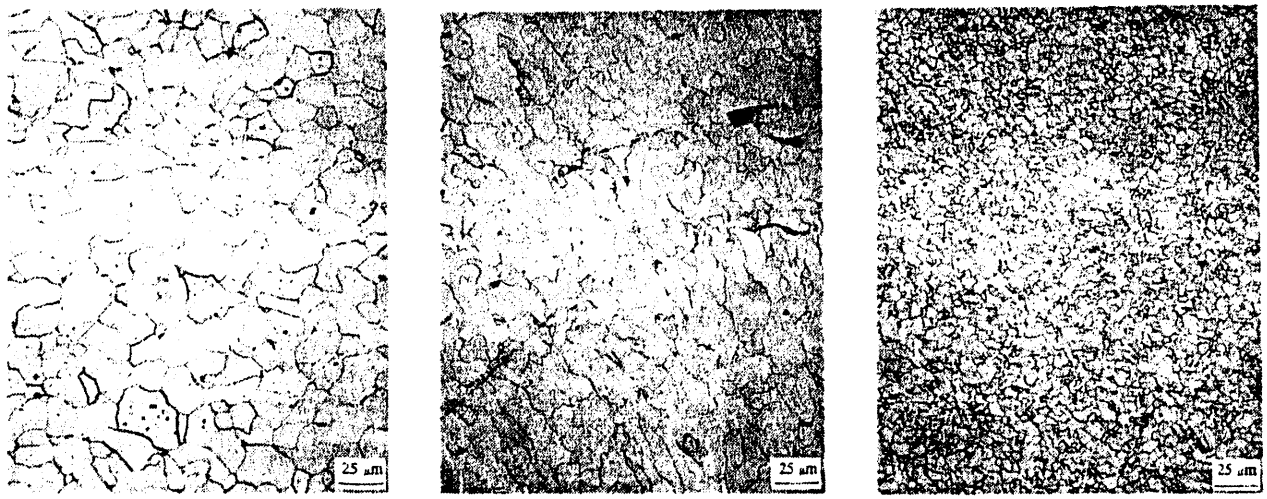

FIG. 10. MICROSTRUCTURES OF COMMERCIAL SAE 1008 HOT BAND (LEFT), AS-DEPOSITED SPRAY-FORMED STRIP (CENTER), AND HOT-ROLLED SPRAY-FORMED STRIP (RIGHT).

TABLE 1. TENSILE PROPERTIES OF COMMERCIAL SAE 1008 HOT BAND AND INEL SPRAY-FORMED AND HOT-ROLLED STRIP.

Sample	Yield Strength 0.2% Offset, MPa (ksi)	Ultimate Strength, MPa (ksi)	Elongation, % in 50 mm	Diamond Pyramid Hardness, 100 g Loads
Commercial 1008 Hot Band	197 (28.6)	306 (44.4)	51.8	91
INEL Spray-Formed and Hot-Rolled, Various Conditions	290-324 (42.0-47.0)	334-498 (48.4-72.3)	13.9-37.7	136-160

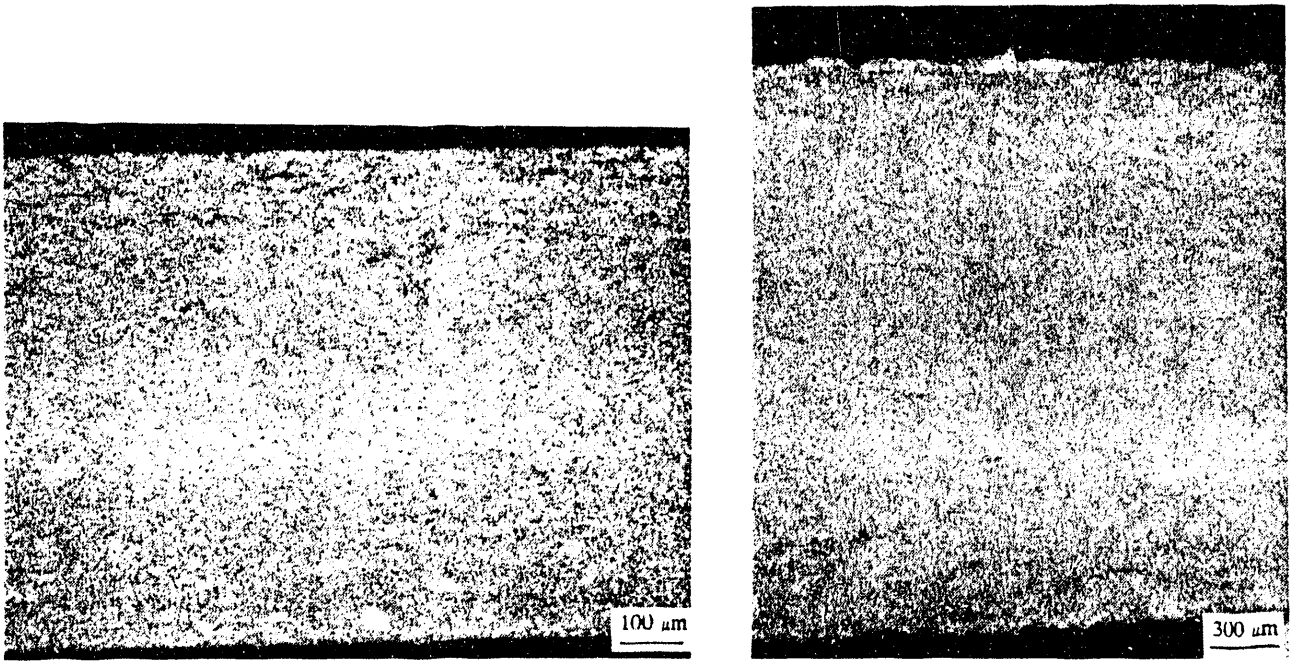

FIG. 11. CROSS SECTION OF THIN SPRAY-FORMED AND HOT-ROLLED STRIP.

underwent the expected grain growth, with a notable decrease in tensile strength and hardness and an increase in ductility.

Polymer Membranes

The transport properties of membranes depend on the membrane's microstructure or "fabric" as well as the physico-chemical properties of the polymer and the operating conditions [23]. The microstructure, in turn, is dictated by the fabrication method.

The need to fully exploit the potential of existing membrane materials through performance-enhancing fabrication techniques is underscored by the increasingly stringent requirements for air and water purity and waste minimization (see, for example, Title I of the Clean Air Act) [24]. To this end, spray-forming technology using de Laval nozzles developed for metal coatings was adapted to polymer membrane fabrication. Membranes were spray formed from poly[bis(phenoxy)phosphazene] (PPOP), an inorganic polymer exhibiting exceptional stability in the adverse thermal (>100°C) and chemical (extreme pH) environments frequently encountered in industrial separations [25].

The gas/gas separation performance of spray-formed membranes compared favorably with that of similar membranes produced by the conventional method of evaporative knife-casting [26]. Membrane fabrication via spray forming was also found to offer advantages in time savings and production flexibility.

Membranes were formed by depositing atomized droplets of linear PPOP dissolved in tetrahydrofuran (THF) onto glass substrates. The chemical stability of the polymer allowed the membranes to be sprayed in air; argon was the atomizing gas. The linear converging-diverging (de Laval) nozzle, designed at the INEL, was machined from boron nitride.

A 7 wt% solution of linear PPOP in THF was sprayed. The weight average molecular weight of the polymer, measured by gel permeation chromatography, was about 750,000 amu. The solution was warmed to ~45°C to lower its viscosity and poured into the tundish of the nozzle, which operated at a static pressure of 137 kPa (20 psia). The solution was aspirated into the nozzle through six small orifices. Solution throughput was about 0.4 kg/s per meter of nozzle throat width. The corresponding gas-to-polymer-solution mass ratio was about 4. Solvent molecules were shed from the atomized droplets during their flight, and the remainder of the molecules evaporated at the substrate. While control of atomizing gas temperature could be a convenient means of adjusting solvent evaporation rate, room temperature argon was used because the equilibrium vapor pressure of THF (145 torr at 20°C) is high enough to allow facile evaporation of the solvent. Upon impact, individual polymer molecules within adjacent droplets interwove, while shedding any remaining solvent.

The polymer/solvent spray was deposited onto 8.3 x 8.3 cm glass plates, maintained at room temperature, that were swept through the spray plume at rates yielding membranes 1 to 10 μm thick. A typical 5 μm thick membrane was fully dried and consolidated in about 1 s.

The hydrophobic membranes were lifted from the substrate by water immersion, mounted onto a porous test cell support, and edge-sealed using polymer solution. Knife-cast membranes prepared using a standard approach were also floated off their glass substrates into water and mounted onto test cell supports.

Experimental parameters such as nozzle geometry and pressure, average molecular weight of the polymer, viscosity and concentration of the polymer solution, evaporation rate of the

solvent, and distance to the substrate had the greatest effect on the spray plume characteristics. The speed, temperature, and properties of the substrate also influenced the membrane's microstructure.

Gas selectivity was measured using a fully automated mixed gas test cell interfaced to a Hewlett Packard 5190 gas chromatograph [27]. The selectivity of spray-formed and knife-cast PPOP membranes was determined for several acid gas mixtures (10% SO_2/90% N_2, 10% H_2S/90% CH_4, 10% CO_2/90% CH_4). SO_2/N_2 mixtures were used to simulate industrial exhaust, while H_2S/CH_4 simulates well gas. Results are given in Table 2. At 80°C, spray-formed membranes had four times the selectivity of knife-cast membranes, when separating SO_2 from nitrogen; at 130°C, the difference increased to about 42 times. Spray-formed membranes had twice the selectivity of similar knife-cast membranes, when separating H_2S from methane at 80°C, and had 67 times the selectivity at 130°C. Improvements were also observed with spray-formed membranes when separating CO_2/CH_4 mixtures.

Membrane fabrication via spray forming offers time savings, flexibility, and improved performance over traditional approaches, e.g., knife casting or spin casting. Whereas knife-cast membrane preparation required hours, spray-formed membranes were prepared in seconds. The flexibility gained by spray-forming membranes to near-net shape not only greatly reduces production costs by eliminating unit operations, but also allows membranes with complex shapes, which are difficult or impossible to manufacture by conventional approaches, to be produced in a straightforward manner. The ability to tailor membrane microstructure to specific separation processes by varying the spray and substrate parameters mentioned previously enhances performance.

TABLE 2. Table 2. Component Selectivity Data for Spray-Formed and Knife-Cast PPOP Membranes.

Gas Mixture	Temperature (°C)	Selectivity: Spray-Formed PPOP	Selectivity: Knife-Cast PPOP
10% SO_2/90%N_2	80	71:1	18:1
10% H_2S/90% CH_4	80	15:1	7:1
10% $C0_2$/90% CH_4	80	4.5:1	3.5:1
10% SO_2/90% N_2	130	344:1	7.2:1
10% H_2S/90% CH_4	130	303:1	5:1

Spray-Formed Tooling

The recent explosion of interest in rapid prototyping technology is fueled in part by the restructuring of today's marketplace. Successful competition in global markets will require the ability to carry a design concept through the prototype stage to production faster and at lower cost than ever before. The ability to generate plastic and wax models of prototype parts with high dimensional accuracy via selective laser sintering [28], stereolithography [29], and other approaches is now a reality. However, it is generally accepted that the rapid production of prototype parts from engineered materials--materials that will actually see service--is the prime long-term goal [30]. Methodologies that can rapidly produce specialized tooling, such as molds and dies, would satisfy this goal, when used with conventional approaches such as injection molding, compression molding, and die casting.

Presently, making complex molds, dies, and related tooling is expensive and time-consuming. Such items can easily cost $200 K apiece and require months to fabricate. Researchers at the INEL have recently begun to develop spray-forming technology to produce specialized tooling by spray depositing molten metal droplets onto patterns made from plastics, waxes, clay, and other easy-to-form materials. This approach could provide a unique opportunity for simplifying production of complex tooling, thereby substantially reducing cost. Rapid solidification enables patterns made from plastics, waxes, clays, etc., to be used despite their low softening temperatures, while near-net-shape capability allows objects with complex shapes to be made easily.

To form a mold, die, etc., liquid metal was pressure-fed into a linear de Laval nozzle transporting high-velocity (mach number ~ 1.5) heated above the liquidus temperature of the metal to be sprayed. Finely atomized metal droplets were entrained in a directed two-phase flow, quenched, and deposited onto a moving plastic pattern having the desired shape and surface texture. The main spray-forming components (spray nozzle, liquid metal reservoir, gas heater, and pattern) were housed in an argon-purged chamber to limit detrimental effects of oxide formation. All spray components were designed and constructed in-house. Bench-scale nozzles having transverse throat widths of 17 mm were typically operated at gas-to-metal mass ratios (for tin) of approximately 10, with metal throughputs of about 0.5 kg/s per meter of nozzle throat width.

At the time of this publication, several low melting point alloys of zinc and tin have been tested with very encouraging results. An example is given in Figure 12, which shows a metal mold produced in about 5 minutes by spray forming molten tin on a plastic (low-density polyethylene) pattern having a butterfly shape. The pattern was not damaged despite the fact that the temperature of the molten metal within the crucible (300°C) greatly exceeded the melting point of the pattern (~100°C). Replication of surface features, including fine scratches in the pattern, was excellent. The surface of the mold was mirror-like and free of solidification shrinkage defects, indicating that replication of the pattern's surface texture also was very good. Patterns of a variety of other plastics, including acrylic, polycarbonate, and polystyrene, have also given good results.

The as-deposited grain structure of a sectioned mold was equiaxed with a fairly narrow range of fine (~6-16 μm) grain sizes--much finer than the massive grains found in cast objects. As-deposited density, measured by water displacement using Archimedes' principle, was typically 88 to 95% of theoretical density.

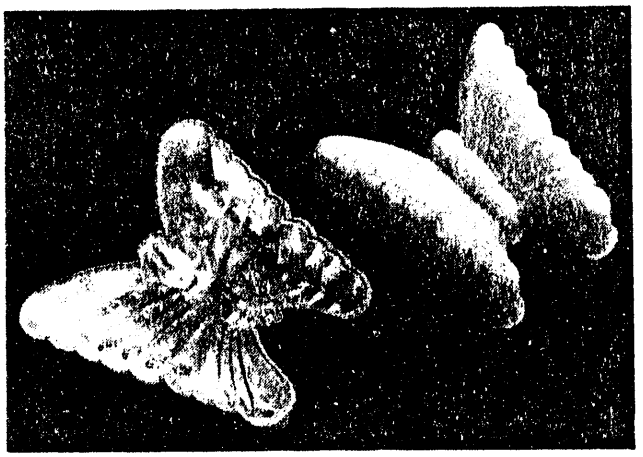

FIG. 12. METAL MOLD SHELL (LEFT) WAS PRODUCED IN ABOUT 5 MIN BY SPRAY DEPOSITING TIN ON A PLASTIC PATTERN (RIGHT).

An important advantage of spray forming molds, dies, etc., is the ability to use patterns made from easy-to-shape materials such as plastic, wax, or clay, even though the softening point of these materials may be well below the crucible temperature of the molten metal. Since plastic and wax prototype models can now be produced using CAD-based systems, spray forming could develop into a complementary approach for generating specialized tooling for manufacturing prototype parts from engineered materials. The reduced fabrication time and cost of these molds/dies would allow rapid design verification and enable new designs and technology to more quickly enter the marketplace.

ACKNOWLEDGMENTS

We gratefully acknowledge significant contributions of Ray Berry in modeling multiphase flow behavior, heat transfer, and solidification phenomena; of Denis Clark in substrate development, process control, and modeling efforts in spray deposition; of James Fincke and David Swank in particle and gas flow field diagnostics; and of Eric Peterson in membrane characterization and testing. This work was supported by the U.S. Department of Energy, Office of Conservation and Renewable Energy, Office of Industrial Technology, and by the EG&G Idaho Laboratory Directed Research & Development Program under DOE Idaho Field Office Contract DE-AC07-76ID01570.

REFERENCES

1. J. F. Key, R. A. Berry, D. E. Clark, J. R. Fincke, and K. M. McHugh, *Development of a Spray-Forming Process for Steel, Final Program Report, December 1991* (Grant No. DE-AC07-76ID01570).

2. A. H. Lefebvre, *Atomization and Sprays*, S. Tamburrino and M. Prescott (eds.), Hemisphere, New York, NY 1989.

3. R. E. Luna and W. A. Klikoff, Jr., *On Aerodynamic Breakup of Liquid Drops*, Sandia Laboratory Report, SC-RR-66-2716, June, 1967.

4. M. Pilch and C. A. Erdman, *Int. J. Multiphase Flow*, **13** (6), 741 (1987).

5. J. L. Beal et al., *Dispersal of Reactor Core Materials by Re-entry Processes*, Cornell Aeronautical Laboratory Reports, 110-900-1, (1964), and 114-080-2, (1965).

6. O. G. Engel, *J. Research N. B. S.*, **60**, 245, (1958).

7. A. R. Hanson, E. G. Domich, and H. S. Adams, *An Experimental Investigation of Impact and Shock Wave Breakup of Liquid Drops*, U. of MN. Inst. of Tech, Rosemont Aeronautical Labs., Final Report to U.S. Bur. of Aeronautics, (1955).

8. A. R. Hanson, E. G. Domich, and H. S. Adams, *Phys. of Fluids*, **6**, 1071, (1963).

9. D. C. Blanchard, *Observation on the Behavior of Water Drops at Terminal Velocity in Air*, GE-OR-7, Project Cirrus, General Electric Res. Lab., (1948).

10. D. C. Blanchard, *Experiments with Water Drops and the Interaction Between Them at Terminal Velocity in Air*, GE-OR-17, Project Cirrus, General Electric Res. Lab., (1949).

11. D. C. Blanchard, *Trans. Am. Geo. Un.*, **31**, 836, (1950).

12. R. L. Koenig, *J. Atmos. Sci.*, **22**, 448, (1965).

13. W. R. Lane, W. C. Prewett, and J. Edwards, *Some Experiments on the Shatter of Drops by Transient Blasts of Air*, Porton Technical Paper, 115, (1949).

14. W. R. Lane, *Ind. Eng. Chem.*, **43** (1), 312, (1951).

15. J. E. Nicholson and B. D. Figler, *Complementary Aerodynamic Test Techniques for Rain Erosion Alleviation Studies*, Paper 66-766, AIAA Aerodynamic Testing Conf., Los Angeles, CA, Sept. 21-23, 1966.

16. E. Rabin and R. Lawhead, *The Motion and Shattering of Burning Propellant Droplets*, Rocketdyne Report, AFOSR TN, 59, (1959).

17. E. Rabin, A. R. Schallenmuller, and R. B. Lawhead, *Displacement and Shattering of Drops by Air Blasts*, Rocketdyne Report, AFOSR TR 60-75, (1960).

18. J. D. Wilcox, R. K. June, H. A. Brown, Jr., and P. G. Kelley, Jr., *J. Appl. Polymer Sci.*, **5**, 1, (1961).

19. H. E. Wolfe and W. H. Anderson, *Kinetics, Mechanisms, and Resultant Droplet Sizes of the Aerodynamic Breakup of Liquid Drops*, Aerojet-General Corp., Report 0395-04(18)SP, (1964).

20. F. C. Haas, *AICHE J.*, **10**, 920, (1964).

21. J. O. Hinze, *AICHE J.*, **1** (3), 289, (1955).

22. A. Ünal, *Intnl. J. Powder Metall.*, **26** (1), 11, (1990).

23. R. R. McCaffrey and D. G. Cummings, *Separation Science and Technology*, **23** (12 & 13), 1627, (1988).

24. *Spectroscopy*, **6** (9), 24, (1991).

25. S. A. Leeper, et al. *Membrane Technology and Applications: An Assessment*, EGG-2282, U.S. DOE Contract No. DE-AC07-76ID01570, February 1984.

26. To be published in *J. Membrane Sci.*

27. E. S. Peterson, M. L. Stone, R. R. McCaffrey, and D. G. Cummings, *Separation Science and Technology* (in press).

28. C. R. Deckard, *Manufacturing Processes, Systems, and Machines: 14th Conference on Production Research and Technology*, S. K. Samanta (ed.), NSF, Ann Arbor, MI, 1987.

29. L. E. Weiss, E. L. Gursoz, F. B. Prinz, P. S. Fussell, S. Mahalingam, and E. P. Partick, *Manufacturing Review*, **3** (1), 40, (1990).

30. S. Ashley, *Mechanical Engineering*, **113** (4), 34, (1991).

DATE
FILMED
7/13/93